

Research Article

Virtual Inertial Control of Small- and Medium-Sized Wind Turbines on Mobile Offshore Platforms with DC Microgrids

Ruifang Zhang,^{1,2} Guoling Wang ,^{1,2} Zhenyu Li,^{1,2} Fuqiao He,^{1,3} Chenghan Luo,^{1,2} and Wensheng Cao⁴

¹School of Marine Engineering, Jimei University, Xiamen 361021, China

²Fujian Key Laboratory of Naval Architecture and Ocean Engineering, Xiamen 361021, China

³China Classification Society Fuzhou Branch, Fuzhou 350008, China

⁴College of Marine Equipment and Mechanical Engineering, Jimei University, Xiamen 361021, China

Correspondence should be addressed to Guoling Wang; wgl@jmu.edu.cn

Received 14 September 2023; Revised 20 May 2024; Accepted 27 May 2024

Academic Editor: C. Dhanamjayulu

Copyright © 2024 Ruifang Zhang et al. This is an open access article distributed under the Creative Commons Attribution License, which permits unrestricted use, distribution, and reproduction in any medium, provided the original work is properly cited.

The renewable energy mobile offshore platform, which adopts the combined power supply of renewable energy and energy storage, is an important carrier for the development and utilization of marine resources. The randomness of renewable energy generation has a more prominent effect on the bus voltage stability and transient voltage deviation of the power system with small capacity and low inertia. Considering the operation and maintenance characteristics of the offshore platform, a virtual inertia control method for small- and medium-sized wind turbines is proposed. Firstly, by analyzing the characteristics of the renewable energy microgrid of the unattended offshore platform, considering the operating environment with high average wind speed at sea, the mechanical inertia in the wind turbine is selected as the energy source of virtual inertia. The structure of the wind power generation unit is analyzed, and small signal modeling is carried out. A virtual inertia control method based on power droop is proposed, and the rotational inertia and the damping coefficient are obtained from the characteristics of transient and steady-state analysis of the system. Finally, the DC microgrid experiment platform of the offshore platform is constructed, and it is verified that the proposed method makes full use of the characteristics of the offshore platform to enhance system inertia and improve the operational stability of the offshore platform DC microgrid system.

1. Introduction

With the continuous development of marine strategies of various countries, offshore platforms have become an important carrier for exploration, development, and utilization of marine resources [1, 2]. The development of renewable energy power generation makes local energy extraction and sea energy utilization the best way for offshore platforms to obtain electric energy and also provides the possibility for long-term stable operation of offshore platforms [3–5]. The renewable energy power generation units such as wind and photovoltaic, energy storage units, and load units together constitute the offshore platform microgrid system. Renewable energy power generation units, energy storage units, and load units are all connected to the system through power

electronic converters, and the system has the characteristics of high degree of power electronization and low inertia [6]. Considering the access and load characteristics of renewable energy power generation units, the DC bus is selected as the common bus of the system. The DC bus voltage is the key to measure the stability of the system, and the transient voltage deviation is the key performance index [7, 8]. Under the maximum power point tracking (MPPT) control, the renewable energy has an efficient energy capture capability, but it also leads to electrical decoupling of the renewable energy from the system control, which makes the influence of the renewable energy intermittency on the bus voltage stability and transient voltage deviation of the DC microgrid system of the low inertia offshore platform particularly prominent. Therefore, the inertia enhancement control has

become an effective measure to ensure the power supply stability of the offshore platform.

At present, there are many related research studies on inertial enhancement control technology. From the application scenario, it is mainly divided into two categories: grid-connected converter and unit converter [9, 10]. The offshore platform microgrid is a typical island microgrid, and its inertial enhancement control technology is mainly applied to the unit converter. The inertial enhancement control technology is mainly divided into three categories according to the object: renewable energy power generation unit, energy storage unit, and load unit [11]. From the perspective of system transient characteristics, energy storage provides an optimal solution for inertial support energy, which requires additional energy storage equipment or upgrading existing energy storage capacity, increasing input costs while requiring more space and load [12–14]; the realization of system inertia enhancement through load management requires accurate system load model and controllability [15]; therefore, considering the limited area and load of offshore platform and making full use of the characteristics of high average wind speed at sea, it is more economical and applicable to improve the power supply reliability of mobile offshore platform by optimizing the control structure of wind power generation unit, releasing the energy stored in the mechanical link of wind turbine, and effectively suppressing the impact of the output power change of wind power generation unit on the bus voltage when the wind speed changes abruptly [16].

At present, there are many research studies on the inertial control technology of wind power generation unit, which are mainly divided into three categories: increasing energy storage equipment, adjusting maximum power tracking control, and using wind turbine mechanical links [17–21]. In [17], the inertia enhancement control of the system is realized by cascading the wind power generation and the lithium-ion battery pack and adaptively adjusting the power reference; in [18], the energy storage system is installed on the DC bus, and the frequency modulation strategy based on frequency trajectory planning (FTP) is used to reduce the influence of the permanent magnet synchronous wind turbine on the system frequency when the wind fluctuates, so as to provide inertial support for the system. The method of increasing energy storage devices is directly effective for enhancing the inertia of the wind turbine, while for the offshore platform, it is necessary to increase the construction cost and require more space and load. Bastiani and de Oliveira [19] realized virtual synchronous generator control by adaptive MPPT control of type-4 wind turbine to enhance the inertia of wind turbine. Hu et al. [20] proposed an active primary frequency regulation strategy for grid-connected wind farms through predictive information to improve the control performance of primary frequency regulation. The essence is to use early or delayed MPPT to achieve system inertia and transient performance improvement. The control structure of the adjusting maximum power point tracking method is complex, which increases the difficulty of system design and reduces the utilization efficiency of renewable energy. It is

not suitable for the system with high dependence on renewable energy power generation on the offshore platform. Therefore, the rational use of the storage inertia of the mechanical link of the wind turbine is the optimal scheme for the inertia enhancement control of the offshore platform. There are also related research studies on the inertial control method of the mechanical link of the wind turbine. In [21], a frequency droop control scheme of the wind turbine based on rotor speed control is used to improve the support of the wind turbine for frequency. The inertial control is realized by controlling the energy stored in the mechanical link of the wind turbine. The method of enhancing the inertia of the system by releasing the energy stored in the mechanical link of the wind turbine often requires detailed modeling of the wind power generation unit, and the control structure is complex.

In view of the above analysis, based on the operation characteristics of the renewable energy DC microgrid of the offshore platform, such as low power level, low inertia, frequent output power fluctuation, and unattended operation, this paper makes full use of the characteristics of high average wind speed at sea and sufficient energy reserve of the mechanical unit of the wind turbine and combines the structural characteristics of the small direct-drive wind turbine with the control structure of the converter of the power generation unit. A virtual inertia control method that uses the mechanical link of the wind turbine to store energy to enhance the inertia of the system is proposed. The specific arrangements of this paper are as follows: the first part introduces the DC microgrid system of the offshore platform; the second part introduces the sources and characteristics of inertia in the microgrid system; the third part focuses on the analysis of the structure of the small power wind turbine power generation unit and establishes the small signal model of the interface converter; in the fourth part, the virtual inertia method based on power droop is proposed by using the energy stored in the mechanical link of the wind turbine to enhance the inertia of the small wind power generation unit, the influence of virtual inertia and damping parameters in the control structure on the dynamic characteristics and stability of the system is analyzed, and the parameter design criteria are obtained; in the fifth part, the experimental platform of renewable energy DC microgrid system on offshore platform is constructed, the proposed method is verified by experiments, and the experimental results are analyzed and discussed.

2. Renewable Energy DC Microgrid System for Offshore Platforms

The DC microgrid system has various structural forms, among which the single bus structure is the most typical structure, which consists of a bus and several other branches, with simple construction, low cost, and easy expansion. Therefore, in this paper, the renewable energy DC microgrid system of the offshore platform is designed as a single bus structure, as shown in Figure 1.

Small direct-drive permanent magnet wind turbines are used for mobile offshore platforms where large wind

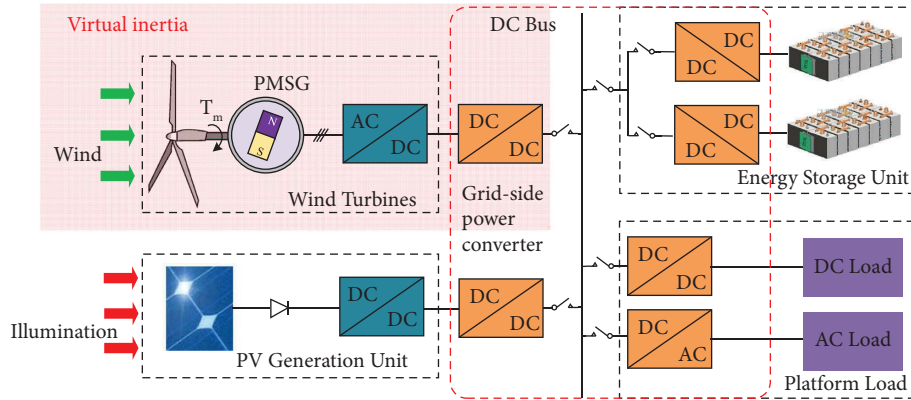


FIGURE 1: DC microgrid system structure of offshore platform.

turbines cannot be installed due to factors such as area, strength, stability, and buoyancy. The system consists of a wind power unit, a photovoltaic power unit, an energy storage unit, a load unit, and a power converter required to connect all units to the DC bus. The wind power unit is connected to the DC bus through a two-stage power converter, with a rectifier circuit at the front and an interface converter at the back for the control of the incoming current. To adapt to the modular requirements, the photovoltaic unit also uses a two-stage converter. The front-stage power converter realizes the maximum power tracking control, and its output is connected to the DC bus via the rear-stage interface converter. The energy storage unit is connected to the DC bus through a DC/DC bidirectional converter, which determines the charging and discharging state according to the bus voltage, achieving bus voltage stability and system power balance. The platform load unit is connected to the DC bus via a DC/DC or DC/AC power converter according to the needs of the power-using equipment.

3. Inertia in Microgrid Systems

In the analysis and design of virtual inertia control links in mobile offshore platform renewable energy DC microgrid systems, the types and sources of inertia in microgrid systems should be analyzed first, and reasonable designs should be made for different systems combined with different extra unit characteristics. The following is an analysis of inertia in microgrid systems based on synchronous units and microgrid systems based on renewable energy sources, providing a theoretical basis for the analysis and design of virtual inertia control links for small wind power units in renewable energy DC microgrid systems on offshore platforms.

3.1. Inertia of Synchronous Machine Microgrid Systems. In a traditional synchronous machine-based AC microgrid system, inertia is expressed as the system's hindrance to frequency changes and is an inherent property of the power system, where the inertia of the system is measured by the inertia constant. The source of inertia of the system is mainly provided by the kinetic energy stored in the synchronously rotating masses (rotor, shaft system, and gears) and is

reflected in the dynamic regulation of power/frequency. For the microgrid system dominated by renewable energy, the system inertia has a richer definition. Its broad form includes the generation-side inertia (synchronous generator inertia), the load-side inertia (motor inertia), and the virtual inertia introduced by the control. The energy source of inertia includes not only the moment of inertia provided by the mechanical rotation link but also the electromagnetic equivalent inertia generated by load optimization control to suppress the voltage fluctuation of the bus and the equivalent inertia generated by virtual inertia control. The composition of each kind of inertia and the relationships between them are shown in Figure 2.

3.2. Inertia of Renewable Energy Microgrid. For the renewable energy-based microgrid, the power generation units are mainly wind power generation units, photovoltaic power generation units, and other renewable energy sources, which have fewer or even no synchronous machines, so the system inertia is low. The inertial characteristics of the renewable energy power generation unit, due to the isolation of the power electronic converter, and the maximum power tracking and control characteristics make the renewable energy intermittent fluctuation quickly transmitted to the bus, affecting the voltage stability of the bus. Depending on the external characteristics of the power converter, the virtual inertia control method is divided into voltage-source virtual inertia control and current-source virtual inertia control. Therefore, for a renewable energy microgrid, its inertia source can be divided into a current source type virtual inertia control unit and a voltage source type virtual inertia control unit. For the renewable energy independent microgrid system of mobile offshore platform, the inertia source is mainly from the renewable energy power generation unit using virtual inertia control of voltage source or current source, except the inertia of synchronous machine. The composition structure is shown in Figure 3. Considering the limited area and load of offshore platforms and the operating environment with high average wind speed at sea, it is critical to effectively use wind power generation units to improve the inertia of renewable energy microgrids on offshore platforms.

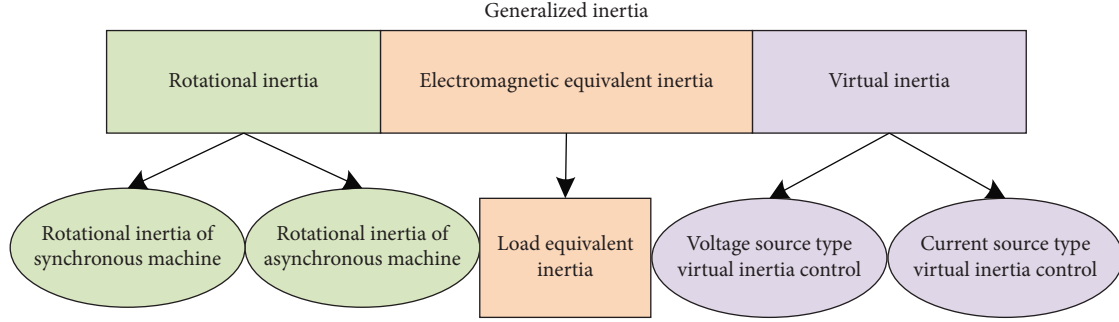


FIGURE 2: Generalized inertia structure composition diagram.

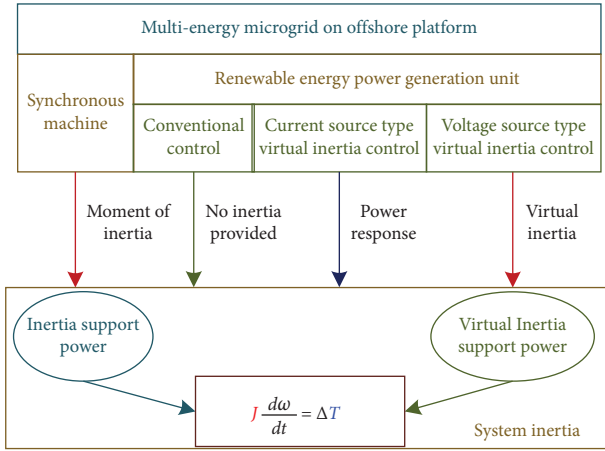


FIGURE 3: Inertia and inertia response of a renewable energy microgrid on an offshore platform.

3.3. Inertia of Wind Power Generation Units. The mobile offshore platform renewable energy independent microgrid is different from other microgrid systems in that the system electrical energy is mainly provided by the wind and light generation units. Its inertia and inertial response are mainly provided by the traditional inertia provided by the wind turbine and the virtual inertia introduced by the control. There is no mechanical link in photovoltaic power generation, and inertia enhancement control can only be achieved by adjusting MPPT or adding storage devices. Due to the existence of mechanical links in the wind power generation unit, the “inertia response” can be achieved by effectively using the energy stored in the mechanical rotation link of the wind turbine to adjust the power transmission characteristics. At the same time, the energy of the inertia response of the wind power generation unit can also be achieved by adjusting the MPPT or energy storage unit storage. The kinetic energy of the rotor is used to achieve the inertial response, while the energy stored in the energy storage unit can be used for both primary frequency modulation and inertial response. Inertia response can be realized by virtual inertia control and droop control, and primary frequency regulation can be realized by pitch angle control and droop control. The structure of the wind turbine inertia response type can therefore be represented as shown in Figure 4.

By comparing the two implementation methods and approaches, it is clear that for the use of additional methods to enhance the inertia of wind power unit, additional energy storage units are required and the cost is high. The self-contained control method is mainly for large-scale wind turbines with adjustable pitch angles. For small- and medium-sized wind turbines on mobile offshore platforms, there is no pitch angle adjustment, and the capacity of the energy storage unit is small due to platform constraints, so virtual inertia control is the best option.

4. Structure Analysis and Small Signal Modeling of Small Wind Power Units

4.1. Structure of Small Wind Turbine Units. The structure of the mobile offshore platform wind power unit used in this paper is shown in Figure 5. The wind turbine is a low-power fixed-pitch wind turbine. The output alternating current of the generator is converted into direct current by diode rectification to reduce energy loss and prevent the formation of reverse current when the output power of the wind turbine is small, so as to realize the inverse power protection of the wind power generation unit. The wind power generation is connected to the DC bus through the interface power converter after rectification.

According to the wind turbine wind energy conversion mechanism, its captured power can be expressed as

$$P_W = \frac{1}{2} \rho \pi R^2 v_{\text{wind}}^3 C_p(\lambda, \beta), \quad (1)$$

where v_{wind} is the wind speed, ρ is the air density, R is the wind turbine blade radius, β is the blade pitch angle, λ is the blade tip wind speed ratio, and C_p is the wind energy utilization factor.

According to Figure 5, the wind power unit consists of a wind turbine, a rotating shaft, and a permanent magnet synchronous generator. The permanent magnet synchronous generator and the wind turbine are rigidly connected through the rotating shaft. When the friction and damping of the rotating shaft are neglected, the mechanical model of the wind power generation system can be simplified as

$$J_{\text{eq}} \frac{d\omega_w}{dt} = T_m - T_e. \quad (2)$$

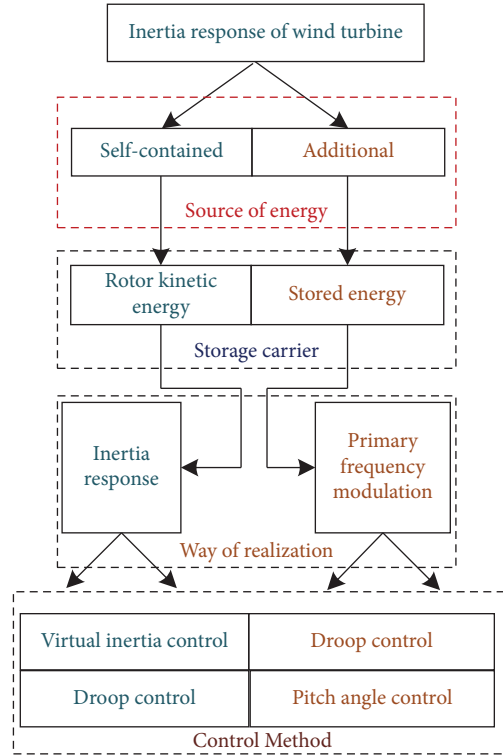


FIGURE 4: Inertia response type of wind turbine.

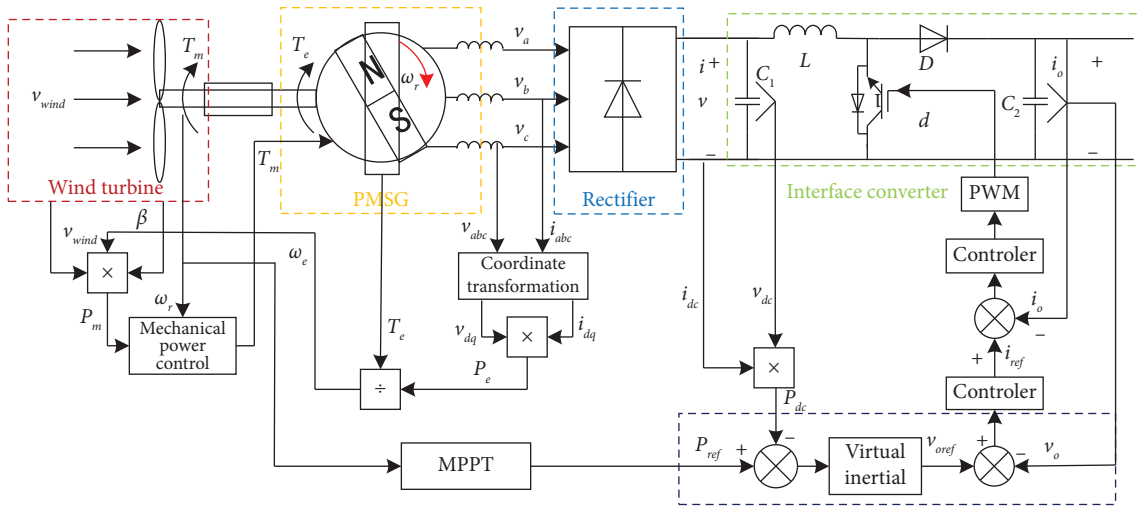


FIGURE 5: Structure diagram of the wind power unit.

Equation (2) is the equivalent rotational inertia of the wind turbine, the rotating shaft, and the synchronous generator, and ω_w is the mechanical speed. T_m is the mechanical torque of the wind turbine, and T_e is the electromagnetic torque of the synchronous generator. According to the wind turbine output mechanical power expression and the power-torque relationship expression, the wind turbine output mechanical torque can be expressed as

$$T_m = \frac{P_m}{\omega_w} = \frac{(1/2)\rho\pi R^2 v_{\text{wind}}^3 C_p(\lambda, \beta)}{\omega_w} \quad (3)$$

P_m is the maximum mechanical power captured by the wind turbine. When the wind turbine is output in steady state, it can be considered that the wind turbine has realized the maximum power tracking; then the wind turbine output power is consistent with the maximum

captured power of the wind turbine, and it can be expressed as

$$P_e = P_W = \frac{1}{2} \rho \pi R^2 v_{\text{wind}}^3 C_p(\lambda, \beta). \quad (4)$$

The rate of change of the electrical state quantity of the synchronous generator is much faster than the rate of change of the mechanical state quantity. To simplify the analysis, the synchronous generator and rectifier are approximated as a whole equivalent to a synchronous torque actuator; then, the electromagnetic torque of the generator is equal to the torque command reference value, as shown in the following formula:

$$T_e = T_{e\text{-ref}}. \quad (5)$$

The output power of the generator is shown in equation (4), so the wind power system is a high-order nonlinear system, and the transfer function expression of the wind power system cannot be derived directly, so the small signal perturbation is used for processing. According to the relationship between torque and power $T = P/\omega_w$, the small signal disturbance is introduced into the system mechanical equation and linearized to give as

$$J_{\text{eq}} \omega_{w0} \frac{d\Delta\omega_{w0}}{dt} = \Delta P_m - \Delta P_e. \quad (6)$$

The mechanical power of the wind turbine P_m is a function of the wind speed v_{wind} and the rotational speed ω_w in equation (6). The partial derivative of P_m gives the expression for the change in mechanical power as

$$\Delta P_m = \left. \frac{\partial P_m}{\partial \omega_w} \right|_{v_{\text{wind0}}} \Delta \omega_w + \left. \frac{\partial P_m}{\partial v_{\text{wind}}} \right|_{\omega_0} \Delta v_{\text{wind}}. \quad (7)$$

Bringing the partial differential term into (7) gives a small perturbation expression for the mechanical power as

$$\Delta \tilde{P}_m = \frac{\lambda_0 C'_{p0}}{C_{p0}} (\Delta \tilde{\omega}_w - \Delta \tilde{v}_{\text{wind}}) + 3 \Delta \tilde{v}_{\text{wind}}. \quad (8)$$

The deviations in (7) and (8), respectively, are expressed as

$$\left\{ \begin{array}{l} \lambda_0 = \frac{R \omega_{m0}}{v_{\text{wind0}}}, \\ C'_{p0} = \frac{dC_p(\lambda)}{d\lambda_0}, \\ \Delta \tilde{P}_m = \frac{\Delta P_m}{P_{m0}}, \\ \Delta \tilde{\omega}_m = \frac{\Delta \omega_m}{\omega_{m0}}, \\ \Delta \tilde{v}_{\text{wind}} = \frac{\Delta v_{\text{wind}}}{v_{\text{wind0}}}, \end{array} \right. \quad (9)$$

where λ_0 , ω_{m0} , P_{m0} , and v_{wind0} are steady-state quantities, and the same small-signal processing and linearization of the output electromagnetic power can give a small perturbation expression:

$$\Delta P_e = \left. \frac{\partial P_e}{\partial \omega_m} \right|_{\omega_{m0}} \Delta \omega_m = \frac{3}{2} \frac{\rho \pi R^5 C_p(\lambda_{\text{opt}})}{\lambda_{\text{opt}}^3} \omega_w^3 \Delta \omega_m. \quad (10)$$

When the system is in steady state, mechanical and electromagnetic losses are neglected, and the electromagnetic power is approximately equal to the mechanical power.

$$\Delta \tilde{P}_e = \frac{\Delta P_e}{P_{m0}} = \frac{3}{2} \frac{\rho \pi R^5 C_p(\lambda_{\text{opt}}) \omega_{m0}^3}{\lambda_{\text{opt}}^3 P_{m0}} \Delta \tilde{\omega}_m. \quad (11)$$

In the steady state, the wind energy utilization factor is the maximum; substituting (8) and (11) into (6), the mechanical equation of the wind energy is derived as

$$J_{\text{eq}} \frac{\omega_m^2}{P_{m0}} \frac{d\Delta \tilde{\omega}_m}{dt} = 3 \Delta \tilde{v}_{\text{wind}} - \frac{3 \rho \pi R^5 C_p(\lambda_{\text{opt}}) \omega_w^3}{2 \lambda_{\text{opt}}^3 P_{m0}} \Delta \tilde{\omega}_m. \quad (12)$$

The mechanical power value at steady state is derived as

$$P_{m0} = \frac{0.5 \rho \pi R^5 C_p(\lambda_{\text{opt}})}{\lambda_{\text{opt}}^3} \omega_{w0}^3. \quad (13)$$

Substituting (13) into (12) and carrying out the Laplace transform, the transfer function of speed fluctuations relative to wind speed fluctuations can be obtained:

$$H(s) = \frac{\Delta \tilde{\omega}_m(s)}{\Delta \tilde{v}_{\text{wind}}(s)} = \frac{1}{1 + \left(\frac{J_{\text{eq}}}{(3 \rho \pi R^5 C_p(\lambda_{\text{opt}}) / 2 \lambda_{\text{opt}}^3) \omega_{m0}} \right) s}. \quad (14)$$

According to equation (10), there is an approximate linear relationship between the output speed fluctuation and the output electromagnetic power in small signal mode. The transfer function of speed fluctuation relative to wind speed fluctuation is further derived as

$$H_p(s) = \frac{\Delta P_e(s)}{\Delta \tilde{v}_{\text{wind}}(s)} = \frac{(2/3) (\lambda_{\text{opt}}^3 / \rho \pi R^5 C_p(\lambda_{\text{opt}}) \omega_{m0}^3)}{1 + \left(\frac{J_{\text{eq}}}{(3 \rho \pi R^5 C_p(\lambda_{\text{opt}}) / 2 \lambda_{\text{opt}}^3) \omega_{m0}} \right) s}. \quad (15)$$

When the wind power generation is running in MPPT control, the inertia time constant of the wind turbine can be approximately derived as

$$T_{\text{MPPT}} = \frac{J_{\text{eq}}}{(3 \rho \pi R^5 C_p(\lambda_{\text{opt}}) / 2 \lambda_{\text{opt}}^3) \omega_{m0}}. \quad (16)$$

According to equations (4)–(16), the response of the system speed and output electric power to fluctuations in wind speed under maximum power tracking control using the optimum blade tip speed ratio is approximated as a first-order inertial link. As the wind turbine system contains mechanical links such as the wind turbine and rotor for power generation, it has some inertia to be able to respond to fluctuations in the input with some inertia. However, for

small direct-drive wind turbines in mobile platform microgrid systems, their rigid connections have less inertia of their own and cannot effectively suppress the impact on the bus voltage when the wind speed changes. Therefore, it is necessary to further enhance the inertia of the wind turbine unit to weaken the impact on the bus voltage during sudden changes in wind speed and improve the system voltage stability.

4.2. Small Signal Modeling of Interface Converter. The wind power unit is connected to the bus through the interface converter. In order to further analyze the characteristics of the wind power generation unit, small signal modeling is needed for the wind power unit interface converter. According to the circuit principle, the DC interface converter can be equated to a two-port network at this time, and the corresponding equivalent circuit structure of the converter is shown in Figure 6.

According to the topological structure of Figure 6, it can be seen that when the switch Q_{wd1} is on, there is

$$\begin{cases} v_{Lwd1} = L \frac{di_{Lwd1}}{dt} = v_{wdin} - R_{Lwd1} i_{wdin}, \\ C_{wd2} \frac{dv_{wdo}}{dt} = -i_{wdo}, \end{cases} \quad (17)$$

and when the switch Q_{wd1} is off, there is

$$\begin{cases} v_{Lwd1} = L \frac{di_{wd1}}{dt} = v_{wdin} - R_{Lwd1} i_{wdin} - v_{wdo}, \\ C_{wd2} \frac{dv_{wdo}}{dt} = i_{wd1} - i_{wdo}. \end{cases} \quad (18)$$

Then the voltage and current balance equation of the converter after averaging it in one switching period is

$$\begin{cases} L_{wd1} \frac{di_{wdin}}{dt} = v_{wdin} - (1-D)v_{wdo} - R_{Lwd1} i_{wdin}, \\ C_{wd2} \frac{dv_{wdo}}{dt} = (1-D)i_{wdin} - i_{wdo}, \end{cases} \quad (19)$$

where R_{Lwd1} is the inductor internal resistance and D is the switching tube steady-state duty cycle. A small signal perturbation of the above equation results in a small signal expression of

$$\begin{cases} (L_{wd1}s + R_{Lwd1})\hat{i}_{wdin} = \hat{v}_{wdin} - (1-D)\hat{v}_{wdo} + \hat{d}V_{wdo}, \\ C_{wd2}s\hat{v}_{wdo} = (1-D)\hat{i}_{wdin} - \hat{d}I_{wdin} - \hat{i}_{wdo}, \end{cases} \quad (20)$$

where \hat{d} is the converter duty cycle disturbance, \hat{i}_{wdin} and \hat{i}_{wdo} are the input and output current perturbations of the interface converter, respectively, \hat{v}_{wdin} and \hat{v}_{wdo} are the input and output voltage perturbations of the interface converter, and I_{wdin} and V_{wdo} are the converter input current and output voltage steady-state values, respectively. Based on the small signal expression and the circuit structure, the transfer

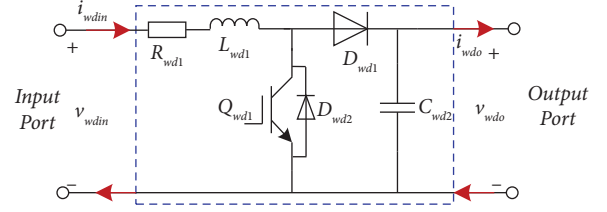


FIGURE 6: Two-port equivalent circuit of the interface converter.

function expression for the input current perturbation to the input voltage can be further obtained as

$$G_{in}(s) = \frac{\hat{i}_{wdin}}{\hat{v}_{wdin}} = \frac{C_{wd2}s}{L_{wd1}C_{wd2}s^2 + R_{Lwd1}C_{wd2}s + (1-D)^2}. \quad (21)$$

The expressions for the transfer function of the input-side current disturbance with respect to the duty cycle and the output current disturbance can be obtained from the equivalent transformation as

$$\begin{aligned} G_{id}(s) &= \frac{\hat{i}_{wdin}}{\hat{d}} = \frac{(1-D)I_{wdin} + C_{wd2}sV_{wdo}}{L_{wd1}C_{wd2}s^2 + R_{Lwd1}C_{wd2}s + (1-D)^2}, \\ G_{ii}(s) &= \frac{\hat{i}_{wdin}}{\hat{i}_{wdo}} = \frac{(1-D)}{L_{wd1}C_{wd2}s^2 + R_{Lwd1}C_{wd2}s + (1-D)^2}. \end{aligned} \quad (22)$$

Then, the transfer function of the output voltage disturbance to the input voltage and duty cycle is

$$\begin{aligned} G_{uu}(s) &= \frac{\hat{v}_{wdo}}{\hat{v}_{wdin}} = \frac{(1-D)}{L_{wd1}C_{wd2}s^2 + R_{Lwd1}C_{wd2}s + (1-D)^2}, \\ G_{ud}(s) &= \frac{\hat{v}_{wdo}}{\hat{d}} = \frac{(1-D)V_{wdo} - (L_{wd1}sI_{wdin} + R_{Lwd1}I_{wdin})}{L_{wd1}C_{wd2}s^2 + R_{Lwd1}C_{wd2}s + (1-D)^2}. \end{aligned} \quad (23)$$

The equivalent output impedance of the converter is expressed as

$$Z_o = \frac{\hat{v}_{wdo}}{\hat{i}_{wdo}} = \frac{-(L_{wd1}s + R_{Lwd1})}{L_{wd1}C_{wd2}s^2 + R_{Lwd1}C_{wd2}s + (1-D)^2}. \quad (24)$$

5. Virtual Inertia Control Method Based on Power Droop and Its Key Parameter Design

5.1. Virtual Inertia Control Method Based on Power Droop. Compared with the traditional generator, the power electronic converter has low inertia. Based on the DC characteristics of the interface converter of the wind power generation unit, the inertia response characteristics of the traditional DC motor are considered to suppress the impact on the system when the input power of the wind turbine changes abruptly, and the inertia response characteristics of the wind power generation unit are improved.

In order to effectively simulate the inertial response of DC motor, it is necessary to analyze its mechanical inertia principle to provide reference for optimizing the controller structure. The DC motor armature equivalent schematic is shown in Figure 7 where r_a is the armature resistance, i_a is the armature current, L_a is the armature winding inductance, E_a is the armature voltage, and v_{dc} is the DC motor-induced electric potential.

Writing the circuit equation for the armature voltage, we obtain

$$E_a = L_a \frac{di_a}{dt} + r_a i_a + v_{dc}. \quad (25)$$

According to the principle of electromagnetic induction in motors, the expression of the induced potential and the angular speed of motor rotation can be expressed as

$$E_a = k_p \omega. \quad (26)$$

From equation (26), it can be seen that the induced electric potential is linearly proportional to the angular speed of motor rotation.

In order to ensure the good tracking of the voltage and current of the output port of the wind unit, the interface converter adopts double loop control. The voltage reference value of the voltage control loop is generated by the power outer loop of the droop control, and its equivalent equation can be expressed as

$$V_{ref} = V_o - k_w (P_o - P_{ref}). \quad (27)$$

The equation for the mechanical speed of a motor in relation to its power can be expressed as

$$J \omega_N \frac{d\omega}{dt} = P_m - P_e - D(\omega - \omega_N), \quad (28)$$

where P_m and P_e are the input mechanical power and output electromagnetic power of the motor, respectively, J is the rotational inertia, ω_N is the rated angular speed of the DC motor, ω is the angular speed of the rotor movement, and D is the damping factor.

By comparing the equivalent equation of the interface converter power control with the armature voltage equation, it can be seen that the two expressions have certain similarities. Therefore, by adding a motor mechanical link to the interface converter power control link to simulate the motor inertia link, the power converter can equate the inertia response externally, thus effectively reducing the impact of the wind power unit output power fluctuation on the system stability.

Therefore, if a virtual inertia control link is added to the control structure of the wind power unit interface converter, part of the control structure is shown in Figure 8.

After the virtual inertial control is embedded into the wind turbine control, the control structure of the wind power generation unit is shown in Figure 9.

After the virtual inertia control is added, the transient response speed of the power loop is much lower than that of the voltage and current loop due to the influence of the

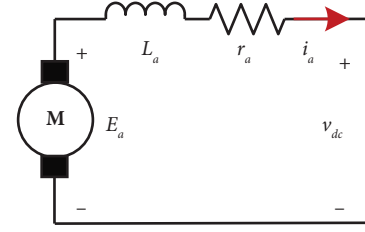


FIGURE 7: Schematic diagram of the armature of the motor.

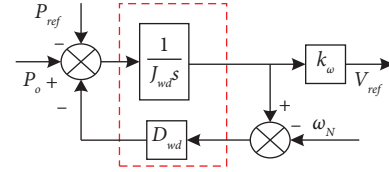


FIGURE 8: Structure diagram of the converter virtual inertia control.

virtual inertia link. At this time, the dynamic process of the interface converter is approximately the dynamic process of the power loop. Therefore, there is

$$\frac{\Delta \hat{v}_o}{\Delta \hat{P}_o} = \frac{1}{J_{wd}s + D_{wd}}. \quad (29)$$

Combined with the inertia characteristics of wind turbine, there is

$$\begin{aligned} H'(s) &= \frac{\Delta \hat{v}_o(s)}{\Delta \hat{v}_{wind}(s)} \\ &= \frac{1}{1 + \left(\left(J_{eq} / \left(3\rho\pi R^5 C_p(\lambda_{opt}) / 2\lambda_{opt}^3 \right) \right) \omega_{m0} \right) s} \frac{1}{J_{wd}s + D_{wd}}. \end{aligned} \quad (30)$$

When the virtual inertia control satisfies (31), the dynamic response of the wind power generation system is dominated by the characteristics of the wind turbine.

$$\frac{J_{wd}}{D_{wd}} \ll \frac{J_{eq}}{\left(3\rho\pi R^5 C_p(\lambda_{opt}) / 2\lambda_{opt}^3 \right) \omega_{m0}}. \quad (31)$$

The inertia time constant of wind power generation is approximately

$$T_{vi} = \frac{J_{eq}}{\left(3\rho\pi R^5 C_p(\lambda_{opt}) / 2\lambda_{opt}^3 \right) \omega_{m0}}. \quad (32)$$

When the virtual inertia control satisfies (33), the dynamic response of the wind power generation system is dominated by the

$$\begin{aligned} &4 \cdot \frac{J_{eq}}{\left(3\rho\pi R^5 C_p(\lambda_{opt}) / 2\lambda_{opt}^3 \right) \omega_{m0}} \\ &\geq \frac{J_{wd}}{D_{wd}} \geq \frac{1}{4} \cdot \frac{J_{eq}}{\left(3\rho\pi R^5 C_p(\lambda_{opt}) / 2\lambda_{opt}^3 \right) \omega_{m0}}. \end{aligned} \quad (33)$$

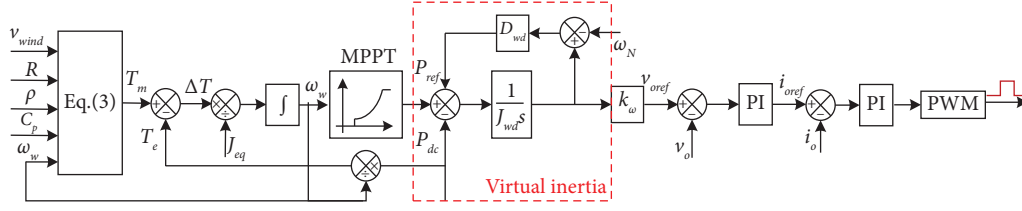


FIGURE 9: Control diagram of the wind power unit interface converter.

When the virtual inertia control satisfies (34), the dynamic response of the wind power generation system is dominated by the characteristics of the interface converter.

$$\frac{J_{wd}}{D_{wd}} \gg \frac{J_{eq}}{(3\rho\pi R^5 C_p(\lambda_{opt})/2\lambda_{opt}^3)\omega_{m0}}. \quad (34)$$

The inertia time constant of wind power generation is approximately

$$T_{vi} = \frac{J_{wd}}{D_{wd}}. \quad (35)$$

From the above analysis, it can be seen that the key to improving the inertia characteristics of wind power generation units through virtual inertia control method is the design of key parameters J_{wd} and D_{wd} , and the steady-state characteristics of the system introduced by the virtual inertia link need further analysis.

5.2. Key Parameter Design Method. In order to further analyze the design principles of the key parameters J_{wd} and D_{wd} of the virtual inertia control and the influence of the virtual inertia control on the stability characteristics of the system, according to the transfer function of the small signal model of the converter and the control structure diagram, the small signal model diagram of the converter control including the virtual control is shown in Figure 10.

According to Figure 10 and the transfer function expression, the closed-loop transfer function of the converter output voltage to the power disturbance can be obtained as

$$G_{vp-vir} = \frac{\hat{v}_o}{\hat{P}_o} = \frac{k_w G_{wdv} G_{ud} G_{wdi}}{(J_{wd}s + D_{wd})(V_m + G_{id} G_{wdi} + G_{wdv} G_{ud} G_{wdi})}. \quad (36)$$

According to the transfer function of output voltage and power, the rotational inertia and the damping factor are in the denominator and therefore have an important influence on the dynamic and steady-state characteristics of the converter response. The higher the damping factor for the generator, the stronger the damping effect of the motor on the oscillations, the better the power response of the motor, and the more stable the system. However, for the control of the power converter, the virtual inertia and damping is not as good as it could be, so it needs to be designed and selected in conjunction with the requirements of the system and the stability of the power converter control.

According to the control structure and the small signal transfer function of the converter control, the rotational inertia J_{wd} and the damping coefficient D_{wd} are the key parameters of the control structure. Therefore, to further optimize the design of these two key parameters, the influence of the key parameters on the output characteristics of the converter needs to be analyzed and determined.

Firstly, the influence of two parameters on the sensitivity of bus voltage to power fluctuation is analyzed. By drawing the Nyquist curve of the closed-loop transfer function after adding the virtual inertia control, the change trend of the two parameters can be effectively characterized and analyzed. The system parameters used for the analysis and experimental validation are shown in Table 1.

The selection of J_{wd} in the virtual inertia control method is the key to affect the virtual inertia of the system. Considering that the inertial energy source of the method used in this paper is the mechanical energy stored by the wind turbine rotor, the energy released under the premise of ensuring stable operation needs to be taken as the key influencing factor of its design. The relationship between the virtual inertial energy and the mechanical storage energy is shown as follows:

$$\frac{1}{2}J_{eq}\omega_w^2 = \frac{1}{2}J_{wd}\omega^2. \quad (37)$$

When the system state changes, the inertial energy is released as

$$\Delta Q = \frac{1}{2}J_{eq}(\omega_{w0}^2 - (\omega_{w0} - \Delta\omega_w)^2) = \frac{1}{2}J_{wd}(\omega_N^2 - (\omega_N - \Delta\omega)^2). \quad (38)$$

After further simplification,

$$\frac{1}{2}J_{eq}(2\omega_{w0}\Delta\omega_w - \Delta\omega_w^2) = \frac{1}{2}J_{wd}(2\omega_N\Delta\omega - \Delta\omega^2). \quad (39)$$

Considering that the speed fluctuation value is much smaller than the steady-state value of the speed, it can be approximately obtained.

$$J_{eq}\omega_{w0}\Delta\omega_w = J_{wd}\omega_N\Delta\omega. \quad (40)$$

Further available.

$$\frac{J_{wd}}{J_{eq}} = \frac{\omega_{w0}\Delta\omega_w}{\omega_N\Delta\omega}. \quad (41)$$

Considering that $\Delta\omega_w$ should not be too large during the operation of the wind turbine, the value of J_{wd} should not be too large while satisfying (36).

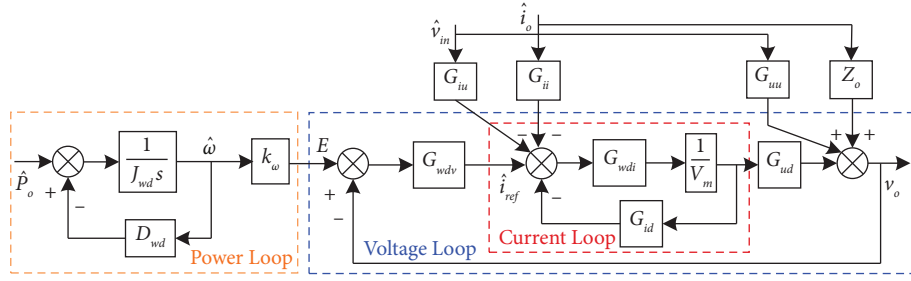


FIGURE 10: Small signal diagram of interface converter control.

TABLE 1: Parameters of the wind unit converter.

Parameter	Symbol	Value
DC bus voltage	V_o	400 V
Output inductance	L_{wd}	$2e-3$ H
Output capacitor	C_{wd}	$500e-6$ F
Virtual rated speed	ω_n	314 rad/s
Moment of inertia	J_{wd}	0.1
Damping coefficient	D_{wd}	100
Sampling frequency	f_s	10 kHz
G_{wdvp} scale factor	k_{wdvp}	0.3
G_{wdvi} integral factor	k_{wdvi}	0.005
G_{wdip} scale factor	k_{wdip}	0.1
G_{wdii} integral factor	k_{wdii}	0.02
Droop coefficient	K_w	2

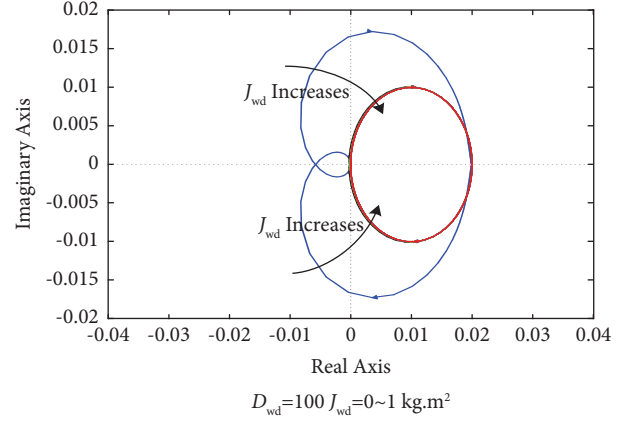
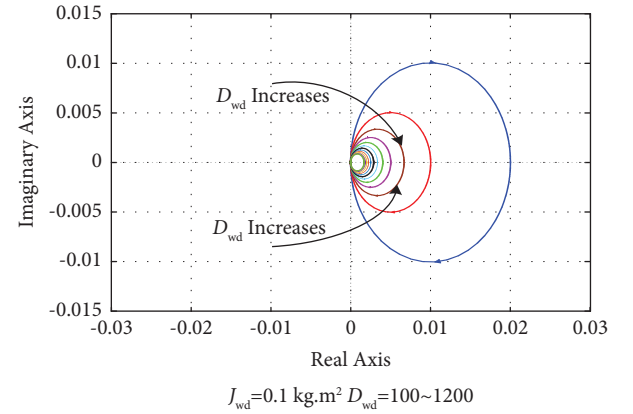
Based on the wind unit interface converter small signal model transfer function and the parameters in Table 1, a Nyquist diagram of the closed-loop transfer function for converter control as the rotational inertia J_{wd} varies with the damping factor D_{wd} can be plotted, as shown in Figures 11 and 12.

As seen from Figure 11, when $D_{wd} = 100$ and the value of J_{wd} varies from 0 to 1, virtual inertia control is used in the converter control link to reduce the sensitivity of the bus voltage to power fluctuations. As J_{wd} increases, the Nyquist curve of the closed-loop transfer function moves away from the unstable region of the left half plane. The Nyquist curve of the closed-loop transfer function of the control system does not enclose the $(-1, j0)$ point, effectively enhancing the stability of the closed-loop control system.

From Figure 12, it can be seen that when $J_{wd} = 0.1$ and $D_{wd} = 100 \sim 1200$, the distance of the Nyquist plot from the left half-plane does not change significantly as the damping factor increases, and the damping factor has no effect on the stability of the voltage at the output port of the converter.

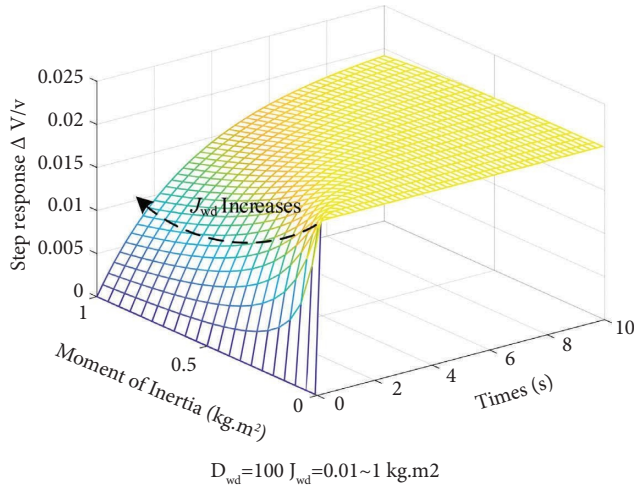
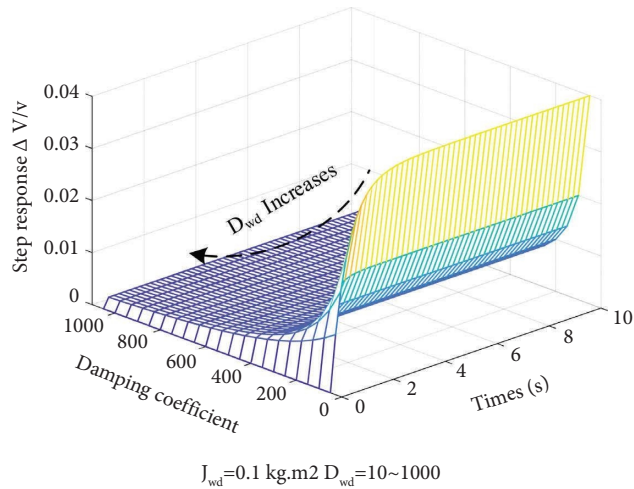
The effect of the virtual inertia link on the transient response of the power converter is further analyzed by using the step response characteristics of the system. This is used to investigate the step response of the port voltage corresponding to different rotational inertia and damping coefficients. Figures 13 and 14 show the step response deviations of the control link for varying rotational inertia and damping coefficients, respectively.

From Figure 13, it can be seen that when $D_{wd} = 100$ and the value of J_{wd} varies from 0.01 to 1, as J_{wd} increases, the response of the closed-loop transfer function slows

FIGURE 11: Nyquist diagram of different J_{wd} closed-loop transfer functions.FIGURE 12: Nyquist diagram of different D_{wd} closed-loop transfer functions.

down and the amount of deviation is smaller, which can better weaken the voltage fluctuations caused by sudden changes in power at the input. However, when J_{wd} is too large, the dynamic response of the system is slowed down, and good dynamic performance cannot be guaranteed. Therefore, the value of J_{wd} should not be too large to ensure a good inertia response and dynamic response speed.

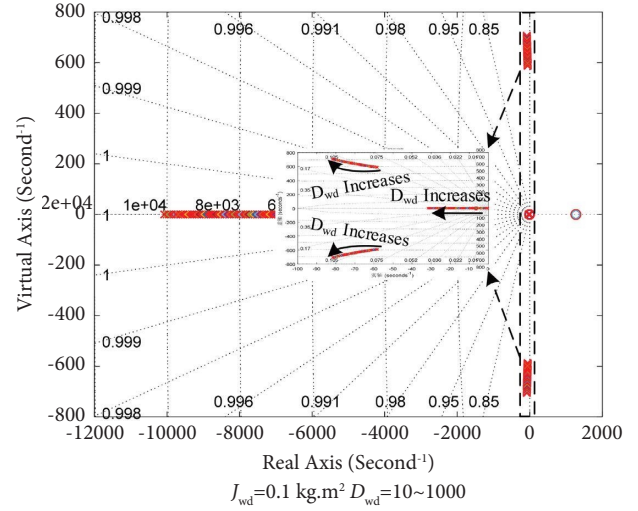
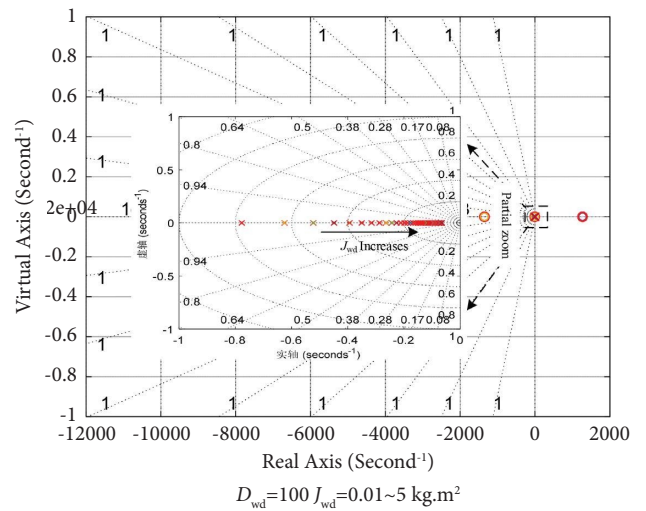
Figure 14 shows that when $J_{wd} = 0.1$ and $D_{wd} = 100$ to 1000, the response time of the converter increases slightly with increasing damping factor, but it does not affect the


 FIGURE 13: Port voltage step response of different J_{wd} .

 FIGURE 14: Port voltage step response of different D_{wd} .

response speed of the system. At the same time, as the damping factor increases, the deviation value of the step response decreases, so the damping factor can also reduce the voltage impact on the output caused by the sudden change in power at the input to a certain extent. According to the linear system stability criterion, the zero-pole distribution of the open-loop transfer function can characterize the stability of the system.

As seen from Figure 15, when $J_{wd} = 0.1$ and $D_{wd} = 100 \sim 1000$, the poles of the transfer function are located in the left half plane, and the system is always stable. As D_{wd} increases, the poles move in the direction away from the imaginary axis, so the higher D_{wd} is, the greater the stability of the converter control system is.

From Figure 16, it can be seen that when $D_{wd} = 100$ and the value of J_{wd} varies from 0.01 to 1, there is a dominant pole in the power converter control system. As J_{wd} increases, the dominant pole of the transfer function moves in the direction of the imaginary axis but is always located in the left half-plane, and the system


 FIGURE 15: Distribution diagram of zero and pole points of transfer function of different D_{wd} .

 FIGURE 16: Distribution diagram of zero and pole points of the transfer function of different J_{wd} .

always remains stable. Therefore, J_{wd} is too large to reduce the response speed of the system, resulting in reduced system stability.

6. Experiment and Analysis

To verify the effectiveness of the proposed control strategy, an experimental platform based on DSP-TMS320F28335 and HIL (hardware-in-the-loop) is used for experimental verification. The composition of the experimental platform is shown in Figure 17. The experiment simulates the intermittent change of wind speed in the offshore platform wind power generation unit and compares the output response of MPPT control and the proposed virtual inertia method when the same wind speed changes. The specific experimental parameters are shown in Table 1.

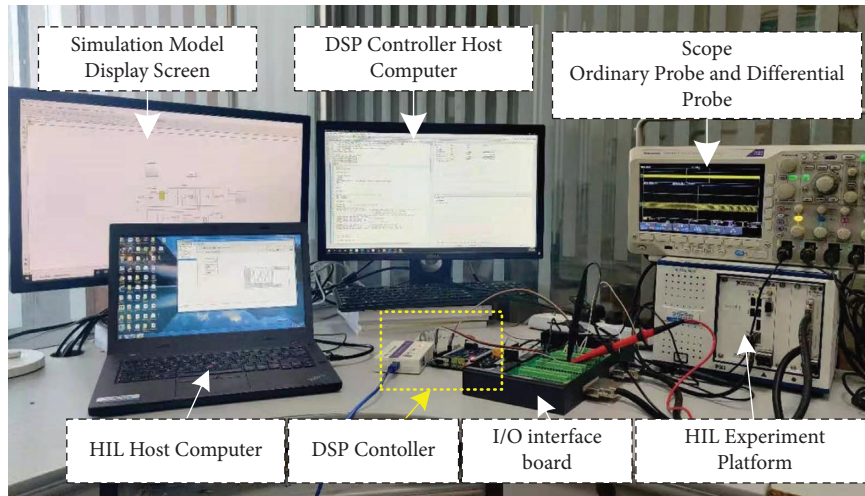


FIGURE 17: Experimental platform.

The HIL is a hardware-in-the-loop simulator, where the hardware-in-the-loop is a real-time processor running a simulation model to simulate the operating state of the controlled object connected to the object under test via the I/O interface. Compared to mathematical simulation, it is closer to the actual situation and is better able to correctly check and debug the performance of the designed controller. The simulator and controller are connected to the measured and controlled objects via an I/O interface board, allowing real-time data interaction between the model and the actual control system, and the experimental results have the advantage of being intuitive and reliable.

Figure 18 shows the experimental waveform of the wind unit port output voltage during intermittent wind speed changes without the virtual inertia link control and with the addition of the virtual inertia control link. The comparison shows that the lack of inertia of the wind turbine itself leads to shocks and oscillations after sudden changes in power during sudden changes in wind speed, reducing the stability of the system. With the addition of the virtual inertia link, the port voltage variation is reduced by 60%, and the response regulation is increased by 0.24 s. This effectively enhances the inertia of the wind turbine and achieves an inertial response, reducing port voltage shocks and improving port voltage stability.

Figure 19 shows the busbar voltage with and without virtual inertia control. The experimental comparison shows that the smaller power of the wind turbine, which accounts for a low proportion of the system capacity, has a smaller impact on the bus voltage during sudden changes in wind speed. However, with the addition of virtual inertia control, the inertia of the wind unit is enhanced. The impact on the bus voltage is reduced by 50%, while the voltage recovery response time is increased by 50%, the bus voltage is smoother, and the power quality is improved.

Figure 20 shows the wind turbine port currents with and without virtual inertia control. The comparison shows that the addition of virtual inertia control to the control link effectively weakens the sudden changes in port current

during power changes. The wind unit output current is smoother, enabling a smooth and orderly injection of energy into the system. Current spikes are also reduced by 50%, and current regulation times are further extended. System stability is enhanced, resulting in a smooth and orderly supply of power to the platform.

Figure 21 shows the variation of the bus current for the two control methods. By comparison, it can be seen that the sudden change in wind output power for the bus current is approximately eliminated by adding the virtual inertia link, and the current changes more smoothly. The reliability of the system power supply has been significantly improved.

To further analyze the effect of adding virtual inertia control on the wind turbine unit, the variation of wind turbine output torque is measured separately for both controls.

Figure 22 shows the variation in the wind turbine output mechanical torque under both controls. The comparison shows that after adding the virtual inertia link to enhance the inertia of the wind unit, the change in torque is smoother when the wind speed changes and the regulation time increases by 66.7%, effectively slowing down the sudden change in output power, achieving an inertial response, avoiding output power oscillations, and improving the performance of the wind turbine.

Figure 23 shows the change in generator output electromagnetic torque under both controls. The comparison shows that the wind unit inertia is enhanced after the addition of the virtual inertia link, and the torque changes more gently when the wind speed changes.

A comparative analysis of the above experimental waveforms shows that the addition of a virtual inertia link to the wind unit interface converter control loop effectively enhances the inertia of the wind unit and achieves an inertial response during sudden changes in wind speed. Compared to the control without the addition of virtual inertia, the wind unit output port characteristics are effectively enhanced, slowing down the rate of power change and effectively suppressing the impact on the busbar. The dynamic

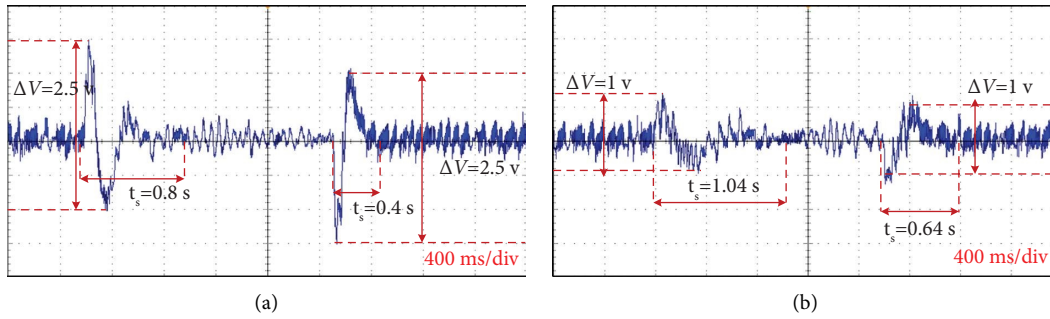


FIGURE 18: Port voltage of the wind unit under two kinds of control. (a) Without virtual inertia control. (b) With virtual inertia control.

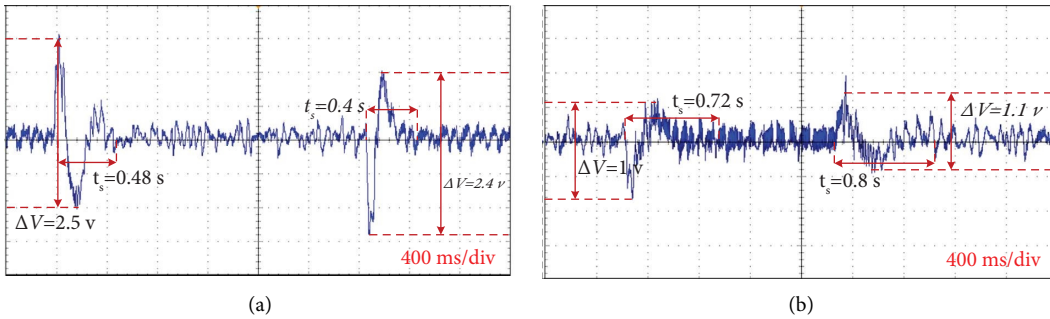


FIGURE 19: Bus voltage of the wind unit under two kinds of control. (a) Without virtual inertia control. (b) With virtual inertia control.

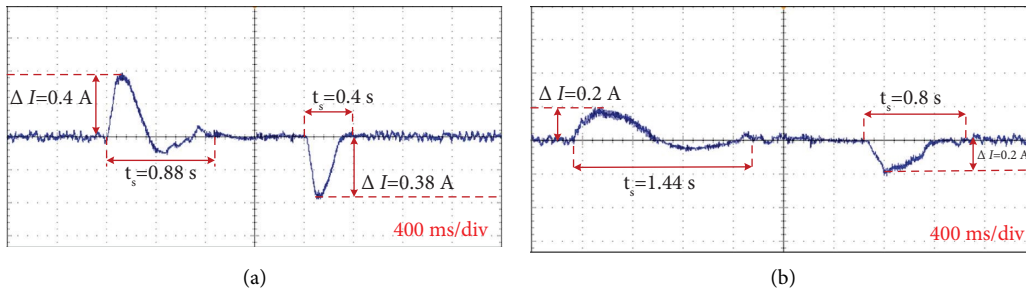


FIGURE 20: Port current of the wind unit under two kinds of control. (a) Without virtual inertia control. (b) With virtual inertia control.

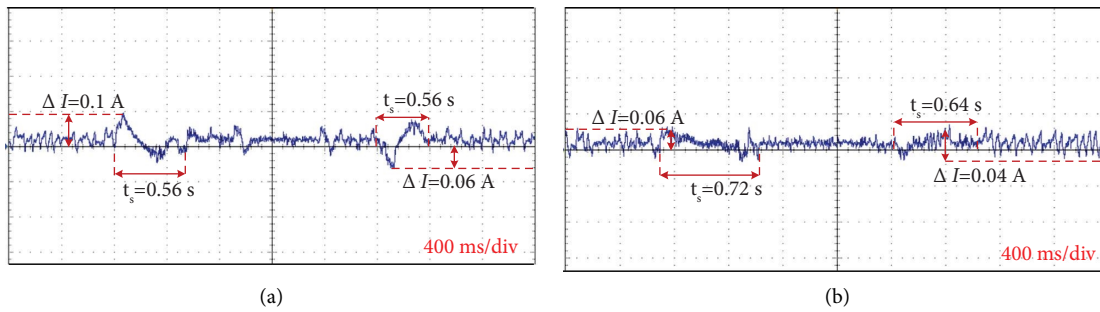


FIGURE 21: The bus current of the wind unit under two kinds of control. (a) Without virtual inertia control. (b) With virtual inertia control.

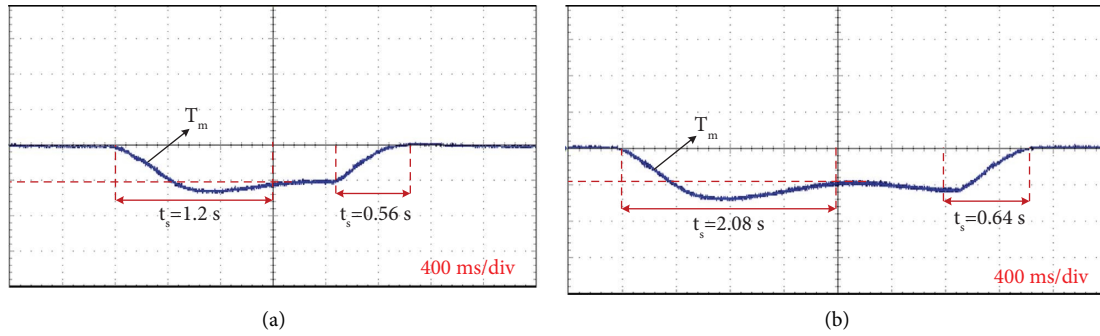


FIGURE 22: Mechanical torque of the wind turbine under two kinds of control. (a) Without virtual inertia control. (b) With virtual inertia control.

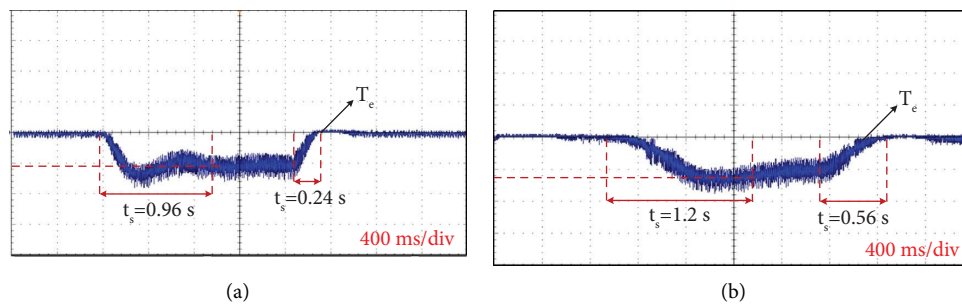


FIGURE 23: Electromagnetic torque of the wind turbine under two kinds of control. (a) Without virtual inertia control. (b) With virtual inertia control.

response of the busbar voltage under intermittent wind speed changes is improved, the power quality is optimized, the reliability of the platform power supply is effectively improved, and the stability of the DC microgrid system of the offshore platform is enhanced.

7. Conclusion

The renewable energy DC microgrid system of mobile offshore platform shows low inertia characteristics due to its small capacity, low inertia, no large power grid, and synchronous generator to provide inertia support. The problem of low stability of DC bus voltage caused by frequent fluctuation of offshore wind speed is particularly prominent. In view of this, the structural characteristics of platform small wind power generation units are analyzed. By combining the interface converter control mechanism with the mechanical structure characteristics of the motor inertial response, the mechanical response of the motor is added to the converter power control loop to achieve virtual inertial control of the wind power unit. The small signal model of the converter control system is established after the virtual inertia control is added, and the structural parameters are analyzed and designed by analyzing the Nyquist diagram of the closed-loop control system and the step response of the system. The following conclusions are obtained through simulation and experimental verification:

- (1) By adding a virtual inertia link to the wind power unit interface converter control loop, the inertia of the wind power unit is enhanced, and the inertia response is achieved during sudden changes in output power, providing inertia support power to the system.
- (2) When the wind speed changes intermittently, the wind turbine as a system with mechanical links can provide a certain inertia. However, due to the small rigidity of the small wind turbine, the impact cannot be completely effectively suppressed. After adding the virtual inertia control, the virtual inertia of the system is enhanced, which effectively suppresses the fluctuation of the bus voltage caused by the intermittent change of the wind speed and improves the stability and power supply reliability of the renewable energy DC microgrid system on the offshore platform.
- (3) The use of virtual inertia control in the converter control loop effectively reduces the shock to the bus voltage caused by intermittent changes in wind speed and enhances system inertia. However, the link changes the main loop of the control structure, increasing inertia damping while also slowing down the system response speed to reasonably select the value of the damping inertia coefficient to ensure dynamic performance and steady-state performance balance.

Data Availability

The data supporting the findings of this study are available within the article.

Conflicts of Interest

The authors declare that they have no conflicts of interest.

Acknowledgments

This work was supported by the National Natural Science Foundation of China (52375065), the Industrial Guidance Project of Fujian, China (2022H0019), the Natural Science Foundation of Fujian, China (2023J01146), and the Youth Science and Technology Innovation Program of Xiamen Ocean and Fisheries Development Special Funds (23ZHQB041QCA06).

References

- [1] C. V. Amaechi, A. Reda, H. O. Butler, I. A. Ja'e, and C. An, "Review on fixed and floating offshore structures part I: types of platforms with some applications," *Journal of Marine Science and Engineering* 10, no. 8 (2022): article 1074, <https://doi.org/10.3390/jmse10081074>.
- [2] E. C. Edwards, A. Holcombe, S. Brown, E. Ransley, M. Hann, and D. Greaves, "Evolution of floating offshore wind platforms: A review of at-sea devices," *Renewable and Sustainable Energy Reviews* 183 (2023): 113416, article 113416, <https://doi.org/10.1016/j.rser.2023.113416>.
- [3] Q. G. Yu, Y. M. Liu, Z. C. Jiang, L. Li, Y. K. Zhang, and M. Guo, "Study of offshore wind power penetration rate in gas turbine generator platform power grid," *Energy Reports* 7 (2021): 141–146, <https://doi.org/10.1016/j.egy.2021.02.011>.
- [4] R. J. Cavagnaro, A. E. Copping, R. Green, et al., "Powering the blue economy: Progress exploring marine renewable energy integration with ocean observations," *Marine Technology Society Journal* 54, no. 6 (2020): 114–125, <https://doi.org/10.4031/mts.54.6.11>.
- [5] M. F. Zia, M. Nasir, E. Elbouchikhi, M. Benbouzid, J. C. Vasquez, and J. M. Guerrero, "Energy management system for a hybrid PV-wind-tidal-battery-based islanded DC microgrid: Modeling and experimental validation," *Renewable and Sustainable Energy Reviews* 159 (2022): article 112093.
- [6] C. Breyer, S. Khalili, D. Bogdanov, et al., "On the history and future of 100% renewable energy systems research," *IEEE Access* 10 (2022): 78176–78218, <https://doi.org/10.1109/access.2022.3193402>.
- [7] K. Jithin, P. Purayil Haridev, N. Mayadevi, R. Pillai Harikumar, and V. Prabhakaran Mini, "A review on challenges in DC microgrid planning and implementation," *Journal of Modern Power Systems and Clean Energy* 11, no. 4 (2023): 1375–1395, <https://doi.org/10.35833/mpce.2022.000053>.
- [8] C. Li, Y. Yang, T. Dragicevic, and F. Blaabjerg, "A new perspective for relating virtual inertia with wideband oscillation of voltage in low-inertia DC microgrid," *IEEE Transactions on Industrial Electronics* 69, no. 7 (2022): 7029–7039, <https://doi.org/10.1109/tie.2021.3100932>.
- [9] Y. Zhang, Q. Sun, J. Zhou, L. Li, P. Wang, and J. M. Guerrero, "Coordinated control of networked AC/DC microgrids with adaptive virtual inertia and governor-gain for stability enhancement," *IEEE Transactions on Energy Conversion* 36, no. 1 (2021): 95–110, <https://doi.org/10.1109/tec.2020.3011223>.
- [10] W. Wu, Y. Chen, A. Luo, et al., "A virtual inertia control strategy for DC microgrids analogized with virtual synchronous machines," *IEEE Transactions on Industrial Electronics* 64, no. 7 (2017): 6005–6016, <https://doi.org/10.1109/tie.2016.2645898>.
- [11] V. Skiparev, R. Machlev, N. R. Chowdhury, Y. Levron, E. Petlenkov, and J. Belikov, "Virtual inertia control methods in islanded microgrids," *Energies* 14, no. 6 (2021): article 1562, <https://doi.org/10.3390/en14061562>.
- [12] H. Tu, H. Yu, and S. Lukic, "Impact of virtual inertia on DC grid stability with constant power loads," *IEEE Transactions on Power Electronics* 38, no. 5 (2023): 5693–5699, <https://doi.org/10.1109/tpel.2023.3243138>.
- [13] E. F. Alves, D. d. S. Mota, and E. Tedeschi, "Sizing of hybrid energy storage systems for inertial and primary frequency control," *Frontiers in Energy Research* 9 (2021): article 649200, <https://doi.org/10.3389/fenrg.2021.649200>.
- [14] T. Kerdphol, F. S. Rahman, M. Watanabe, Y. Mitani, D. Turschner, and H. P. Beck, "Enhanced virtual inertia control based on derivative technique to emulate simultaneous inertia and damping properties for microgrid frequency regulation," *IEEE Access* 7 (2019): 14422–14433, <https://doi.org/10.1109/access.2019.2892747>.
- [15] T. Chen, J. Guo, B. Chaudhuri, and S. Y. Hui, "Virtual inertia from smart loads," *IEEE Transactions on Smart Grid* 11, no. 5 (2020): 4311–4320, <https://doi.org/10.1109/tsg.2020.2988444>.
- [16] R. Zhang, F. He, G. Wang, and Z. Li, "A kind of virtual inertial control of small and medium-sized wind turbines on removable offshore platforms with DC microgrids," in *Proceedings of 2022 IEEE International Power Electronics and Application Conference and Exposition (PEAC)* (Guangzhou, China, June 2022), 351–354, <https://doi.org/10.1109/PEAC56338.2022.9959235>.
- [17] R. K. Tagayi, S. Han, H. Lee, and J. Kim, "Reliable frequency control support scheme based on wind power generator combined with rechargeable energy storage system applying adaptive power reference," *Applied Sciences* 13, no. 9 (2023): article 5302, <https://doi.org/10.3390/app13095302>.
- [18] Y. Qian, H. Wang, M. Zhou, H. Lv, and Y. Liu, "Frequency trajectory planning-based frequency regulation strategy for wind turbines equipped with energy storage system," *Chinese Journal of Electrical Engineering* 8, no. 2 (2022): 52–61, <https://doi.org/10.23919/cjee.2022.000014>.
- [19] B. A. Bastiani and R. V. de Oliveira, "Adaptive MPPT control applied to virtual synchronous generator to extend the inertial response of type-4 wind turbine generators," *Sustainable Energy, Grids and Networks* 27 (2021): article 100504.
- [20] Z. Hu, B. Gao, and R. Sun, "An active primary frequency regulation strategy for grid integrated wind farms based on model predictive control," *Sustainable Energy, Grids and Networks* 32 (2022): article 100955.
- [21] J. Boyle, T. Littler, S. M. Mueyeen, and A. M. Foley, "An alternative frequency-droop scheme for wind turbines that provide primary frequency regulation via rotor speed control," *International Journal of Electrical Power and Energy Systems* 133 (2021).